AIP | The Journal of Chemical Physics

Rotational spectroscopy and three-wave mixing of 4-carvomenthenol: A technical guide to measuring chirality in the microwave regime

V. Alvin Shubert, David Schmitz, Chris Medcraft, Anna Krin, David Patterson, John M. Doyle, and Melanie Schnell

Citation: The Journal of Chemical Physics **142**, 214201 (2015); doi: 10.1063/1.4921833
View online: http://dx.doi.org/10.1063/1.4921833
View Table of Contents: http://scitation.aip.org/content/aip/journal/jcp/142/21?ver=pdfcov
Published by the AIP Publishing

Rotational spectroscopy and three-wave mixing of 4-carvomenthenol: A technical guide to measuring chirality in the microwave regime

V. Alvin Shubert,[1,2] David Schmitz,[1,2] Chris Medcraft,[1,2] Anna Krin,[1,2] David Patterson,[3] John M. Doyle,[3] and Melanie Schnell[1,2,4,a)]
[1]*Max Planck Institute for the Structure and Dynamics of Matter, 22761 Hamburg, Germany*
[2]*The Center for Free-Electron Laser Science, 22761 Hamburg, Germany*
[3]*Department of Physics, Harvard University, Cambridge, Massachusetts 02138, USA*
[4]*The Hamburg Centre for Ultrafast Imaging, Universität Hamburg, 22761 Hamburg, Germany*

(Received 1 April 2015; accepted 18 May 2015; published online 2 June 2015)

We apply chirality sensitive microwave three-wave mixing to 4-carvomenthenol, a molecule previously uncharacterized with rotational spectroscopy. We measure its rotational spectrum in the 2-8.5 GHz range and observe three molecular conformers. We describe our method in detail, from the initial step of spectral acquisition and assignment to the final step of determining absolute configuration and enantiomeric excess. Combining fitted rotational constants with dipole moment components derived from quantum chemical calculations, we identify candidate three-wave mixing cycles which were further tested using a double resonance method. Initial optimization of the three-wave mixing signal is done by varying the duration of the second excitation pulse. With known transition dipole matrix elements, absolute configuration can be directly determined from a single measurement. © *2015 AIP Publishing LLC.* [http://dx.doi.org/10.1063/1.4921833]

I. INTRODUCTION

Chiral effects are ubiquitous in chemistry and biology, manifested in handedness-dependent interactions of chiral objects with their environment. Examples include optical polarimetry,[1] enantioselective chemistry,[2] and a wide range of chirality-dependent biological reactions.[3–5] Both stereochemistry and chiral analysis are active areas of research.[6–13] The development of techniques that offer improved chiral analysis, such as enantiomeric differentiation and enantiomeric excess (*ee*) determination, and a better understanding of chiral interactions, e.g., the interaction of light with chiral molecules, remain important goals. Furthermore, chiral analysis is a key tool for elucidating chiral effects in chemical reactions and biological processes.

Recently, we demonstrated a new technique, chirality-sensitive microwave (MW) three-wave mixing, to identify the enantiomers of chiral molecules and to measure *ee* within gas-phase mixtures.[14–16] The general connection between rotational resonances and chirality, i.e., that resonances within a triad of rotational levels can be used to differentiate enantiomers, was conjectured by Hirota.[17] Applying three-wave mixing within a supersonic jet takes advantage of the cold, collision-free environment of the expansion that allows one to more easily probe the stereochemical structure of individual molecules in a conformation specific manner.

One of the goals of chiral molecule research is to rapidly and unambiguously identify molecular components in complex mixtures. For this aim, microwave three-wave mixing is advantageous because every molecule, and even its conformational isomers and isotopologues, has a unique and easily resolvable rotational spectrum. The essential conditions for applying our method are that each dipole moment component of the chiral molecule is nonzero and that it can be brought into the gas phase.

Herein, we present a beginning-to-end example of applying microwave three-wave mixing to a conformational mixture and also a kind of "handbook" for basic application of the method. Our work here includes measuring and assigning the rotational spectrum of an uncharacterized chiral molecule, identifying three-wave mixing cycles, and analyzing the newly characterized molecule in a chiral mixture. The spectral fitting and subsequent determination of the rotational constants of a previously uncharacterized species are key steps in this process as the rotational constants are compared with quantum chemical calculations to obtain the dipole moment components. The rotational constants and dipole moment components are used to predict candidate three-wave mixing cycles. These closed cycles consist of three transitions that we define as drive, twist, and listen. Due to our particular experimental setup, the drive and listen transitions occur in the MW range and the twist transitions in the radio frequency (RF) range. In general, triads including rotational transitions in any frequency range can be used and three-wave mixing with all three transitions in the MW range has already been demonstrated.[13] Once three-wave mixing cycles have been verified and excitation pulses optimized, careful measurements enable the determination of the absolute configuration and quantification of the *ee*.

A global fit to the observed rotational transitions is not a prerequisite for performing three-wave mixing to differentiate enantiomers and measuring enantiomeric excess. Rather, once a rotational spectrum has been recorded, double-resonance experiments can determine which transitions arise from shared

a)Author to whom correspondence should be addressed. Electronic mail: melanie.schnell@mpsd.mpg.de

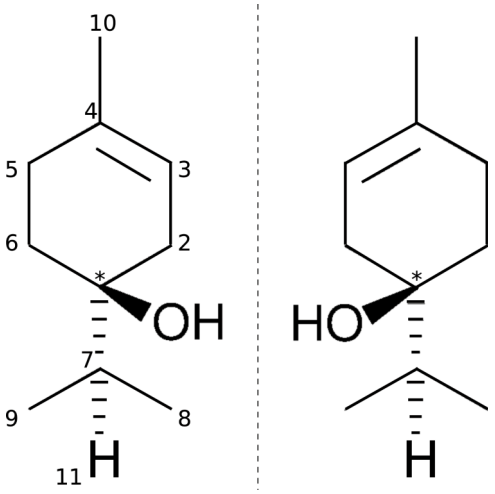

FIG. 1. Chemical structure of 4-carvomenthenol (terpinen-4-ol). The S-enantiomer (+) is on the right while the R-enantiomer (−) is on the left. The chiral center is marked with an asterisk in both structures.

energy levels. Due to their low frequencies, the twist transitions employed herein cannot be directly observed with our spectrometer and must either be predicted from the rotational constants or indirectly determined via double resonance RF-MW experiments.[18] In the future, with more advanced and faster electronics available, it is possible that three-wave mixing could become a technique useful for faster characterization and assignment of observed rotational spectra.

In this work, we use as a prototype example the terpenoid, 4-carvomenthenol (also known as terpinen-4-ol, IUPAC name 4-methyl-1-propan-2-ylcyclohex-3-en-1-ol), shown in Figure 1. It is the major component of tea tree oil,[19] a widely used ingredient in cosmetics and treatment of skin conditions,[20] and a liquid at room temperature. 4-carvomenthenol contains a single stereogenic center and thus exists as one of two enantiomers. The (*R*)-4-carvomenthenol enantiomer is produced with an *ee* > 99% by the male beetle of the scolytid *Polygraphus poligraphus* (L.).[21] It is structurally flexible such that rotations of and within the isopropyl and hydroxyl groups and deformations of the cyclohexene ring give rise to several low energy conformers. Taken together, these facts make 4-carvomenthenol chemically and spectroscopically a very interesting molecule to investigate.

Herein, we first give an overview of the theory underpinning three-wave mixing, then describe the methods, both experimental and computational, used to investigate 4-carvomenthenol. Next, we present the results from the broadband MW spectrum and make structural assignments from comparison between fitted rotational constants and quantum chemical calculations. We present results from MW-RF double resonance experiments to precisely determine the twist transition frequencies and their optimal excitation conditions. Three-wave mixing results are then presented. Finally, we conclude with a discussion of our major findings and an outlook to future challenges and applications.

II. THEORETICAL BACKGROUND

Microwave three-wave mixing is a polarization-dependent double-resonance excitation experiment. Its sensitivity to the phase of the recorded signal enables enantiomeric differentiation.[17] To perform the experiment, a closed cycle of electric dipole transitions connecting three rotational energy levels is required. The sum or difference of the two excitation frequencies is equal to the frequency of the recorded signal, as illustrated in the energy level diagram of Figure 2. The experiment is performed with linearly polarized radiation, such that the

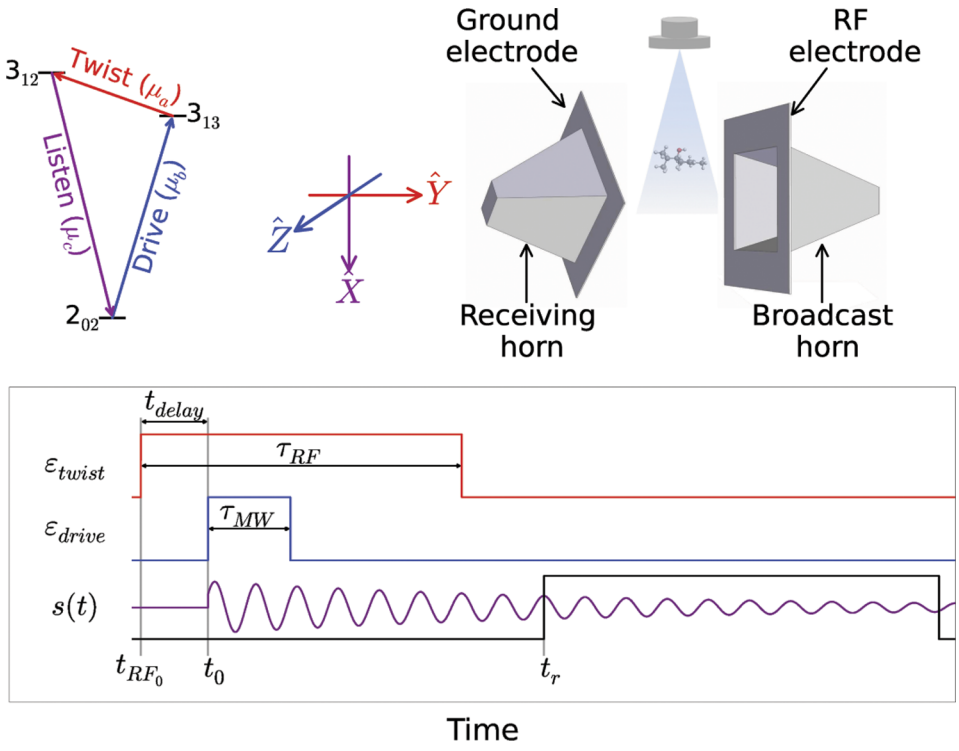

FIG. 2. Overview of the interaction region of the COMPACT spectrometer. Linearly polarized (along Z) MW radiation is broadcast into the chamber with a horn antenna and the molecular response received by a second horn. In three-wave mixing, the electrodes generate a RF field linearly polarized (along Y) perpendicular to the MW radiation and the molecular response is linearly polarized in the third mutually orthogonal direction (along X). The energy level diagram is shown for the three-wave mixing cycles used for 4-carvomenthenol conformers A and C. The timing scheme of the experiment (not to scale) illustrates when the different excitation pulses are present relative to each other in the molecular interaction region. The RF twist pulse starts at t_{RF_0} and has a duration τ_{RF}, the MW drive pulse has a duration τ_{MW} and starts at $t_{RF_0}+t_{delay}$, which coincides with the onset of the three-wave mixing signal at t_0. The recording of the three-wave mixing signal begins at t_r.

excitation pulses (drive and twist) are polarized perpendicular to each other and the signal (listen) is recorded in the third mutually orthogonal direction. Due to the operating range of our instrument, the drive and twist pulses are limited to the MW (2-6 GHz) and RF (50-550 MHz) ranges. Either the drive or the twist can occur in the RF range. However, due to the population difference between levels and the operating powers of the amplifiers (300 W for the MW and 100 W for the RF), it is advantageous for us to drive and twist with the MW and RF pulses, respectively.

Enantiomeric identification arises from the fact that the phases of the time-domain listen signals differ by π radians between the enantiomers. This difference is due to the signal dependence on the product, $\mu_X\mu_Y\mu_Z$, of the transition dipole matrix (TDM) elements in the laboratory frame for each transition, which is of opposite sign between enantiomers. The observed signal has the form

$$s \propto ee \cdot \cos(2\pi\nu t + \phi_{MW} + \phi_{RF} \pm \frac{\pi}{2}(1 + \frac{\mu_X\mu_Y\mu_Z}{|\mu_X\mu_Y\mu_Z|})). \quad (1)$$

Equation (1) is derived from Eq. (16), as described in the supplementary material.[22] We only employ here the derivation for a progressive cycle scheme, i.e., the listen frequency is the sum of the drive and twist frequencies. The expression is the same for a regressive cycle scheme so long as the indices and signs are changed appropriately in Eq. (16) of Ref. 22. In Eq. (1), the excitation pulses are assumed to be on resonance and the drive and twist pulses are at (or less than) π and 2π conditions, respectively. Note that maximum three-wave mixing signal is obtained with a $\frac{\pi}{2}$ drive pulse and a π twist pulse.[13,23] The phase of the listen signal at the start of emission is $\phi_{MW} + \phi_{RF}$, where ϕ_{MW} and ϕ_{RF} are the phases of the drive and twist excitation pulses upon their arrival in the interaction region of the spectrometer.[23] The dependence on the product of the transition dipole matrix elements has been moved inside the cosine expression of Eq. (1) as an additional phase term. Note that the transition dipole matrix elements in the laboratory frame depend upon J, K_a, K_c, and M, where J is the total angular momentum quantum number, K_a and K_c are labels that refer to the symmetric top quantum number K (the projection of J onto the molecular frame z-axis) in the prolate and oblate symmetric rotor limits,[24] respectively, and M is the projection of the angular momentum onto the laboratory frame Z-axis.[25] The observed phases measured at a time, t_r (the time at which free induction decay (FID) recording starts relative to the t_0 of the listen signal emission), are

$$\phi_{obs} = -2\pi\nu t_r + \phi_{MW} + \phi_{RF} \text{ if } \mu_X\mu_Y\mu_Z < 0, \quad (2)$$

$$\phi_{obs} = -2\pi\nu t_r + \phi_{MW} + \phi_{RF} \pm \pi \text{ if } \mu_X\mu_Y\mu_Z > 0. \quad (3)$$

Furthermore, the intensity of the signal is directly proportional to the *ee* and thus allows for a molecule (and even conformer) specific measurement of the *ee*.

III. EXPERIMENTAL AND COMPUTATIONAL METHODS

Three main experiments are performed in this work. First, the rotational spectrum of an uncharacterized molecule is obtained and assigned. Double-resonance experiments are then performed to verify the frequency of the twist transitions within the radio frequency range. Finally, three-wave mixing experiments are performed to identify the absolute configuration of the enantiomer in excess and to determine the magnitude of the enantiomeric excess.

The Hamburg COMPACT spectrometer used for this study has been previously described.[16,26] The original apparatus is detailed in Ref. 26 while the modifications required for the MW-RF double resonance and three-wave mixing experiments are described in Ref. 16.

In broadband rotational spectroscopy, a microwave chirp spanning several GHz in only a few microseconds excites the molecules.[27] In our apparatus, an arbitrary waveform generator (AWG) creates the MW waveforms that are then amplified prior to broadcast into the chamber via a horn antenna. When the molecules are resonant with a frequency within the chirp, a polarization of the molecular ensemble is created. The FID of this polarization is recorded with a second microwave horn. The Fourier transform of this FID from the time to the frequency domain yields the microwave spectrum. The exact length of the recorded FID varies according to both the lifetime of the FID and the final frequency domain resolution required. In experiments performed to characterize a new molecule, the FID is recorded for 50 μs to yield a frequency resolution of 20 kHz. After the transition frequencies are identified and assigned, typically 10 μs of the FID is recorded in further experiments (e.g., the MW-RF double-resonance and three-wave mixing experiments, see below). Shorter FID recording allows us to run at a faster experimental duty cycle. A single FID per valve pulse is recorded in these experiments.

The molecules of interest (*R*)-4-carvomenthenol (Sigma Aldrich ≥95% sum of enantiomers, ~2:1 enantiomeric ratio) and (*S*)-4-carvomenthenol (Sigma Aldrich ≥98.5% sum of enantiomers, ~2:1 enantiomeric ratio) are used without further purification and heated in a sample reservoir to 90 °C. A pulse valve (General Valve Series 9) is used to introduce the molecules into the vacuum chamber via a supersonic expansion. The supersonic expansion cools the molecules to rotational temperatures of around 1-2 K. In some experiments, two valves separated by 3.5 cm (nozzle orifice separation) with opposite enantiomers or mixtures in their respective sample reservoirs are used. In the two-valve arrangement, a digital delay generator (Stanford Research, model DG645) is used to control which valve pulse interacts with the MW and RF excitation pulses within an experimental cycle.

Quantum chemical calculations aid the assignment of structures to the observed spectra and provide estimates of the dipole moment components required for identifying the most promising candidate cycles. The conformational flexibility of 4-carvomenthenol lies in the orientations of the isopropyl and hydroxyl groups with respect to the cyclohexene ring. Intuitively, structures with the hydroxyl hydrogen pointed towards the cyclohexene ring should be preferred due to a stabilizing interaction between the hydroxyl hydrogen and cyclohexene double bond. For this structural moiety, relaxed potential energy scans of rotation of the isopropyl group are performed using the Gaussian 09 suite of programs[28] at the B3LYP/6-311++G(d,p) and M06-2X/6-311++G(d,p) levels of theory.

Additional calculations with the OH hydrogen pointed away from the cyclohexene ring are also performed.

Three-wave mixing candidate cycles are evaluated once a molecule is characterized, i.e., the rotational spectrum is fit (with SPFIT[29]) and assigned to a quantum chemically calculated structure (or structures). Candidate cycles are those with the largest product of predicted line strengths, $I_{p,total} = I_{p,drive} \cdot I_{p,twist} \cdot I_{p,listen}$, where $I_{p,i}$ is the prediction for transition i. The predictions are made with the rotational spectroscopy prediction program, SPCAT,[29] using the experimentally fitted rotational constants and calculated dipole moment components.

As described in our carvone work,[16] the spectrometer is modified to perform the MW-RF double resonance and three-wave mixing experiments. Figure 2 presents a schematic of the interaction region of the modified spectrometer. A set of stainless steel electrodes supports a radio frequency field in the interaction region between the broadcast and receiving horns. The RF waveforms are generated on the same AWG that generates the MW waveforms, thus ensuring phase stability. The RF pulse is amplified (100 W) prior to being coupled to the electrodes. Ideally for performing three-wave mixing with our spectrometer's geometry, the receiving horn should be turned 90° relative to the excitation horn, while it is unrotated for traditional MW experiments. In the three-wave mixing experiments herein, the receiving horn is turned to only 45° relative to the broadcast horn, allowing us to record both traditional MW spectra and the three-wave mixing signals. However, in this geometry, the recorded signal is reduced by a factor of $\sqrt{2}$ because only the component of the signal polarized along the long axis of the receiving horn can be acquired. In the near future, we will install a dual polarization horn that will allow high signal gain from both three-wave mixing and traditional MW measurements.

After identifying candidate cycles, double resonance experiments are performed to validate the predicted radio frequencies, to check the feasibility that adequate signal can be obtained from a given cycle, and to optimize the excitation pulses. The RF is scanned over the region of the predicted twist resonance while monitoring the signal of the listen transition in the MW range. This double-resonance experiment enables the measurement of RF transitions that are otherwise invisible to our spectrometer. Typically, a 2-6 GHz chirp with 1 μs duration is temporally overlapped with the first 1 μs of a 2-5 μs RF pulse, as shown in the timing scheme in Figure 2. At this stage, optimizations of the RF pulse length are made, ideally to achieve a π-pulse.[13,23] If the frequency predictions from the rotational constants are very accurate, only RF pulse duration scans are needed to probe potential cycles and to optimize the excitations. Note that the receiving horn is not rotated relative to the excitation horn in these double-resonance experiments.

Three-wave mixing experiments are performed by broadcasting a linearly polarized single frequency MW pulse (polarized along the laboratory frame Z-axis, see Figure 2) into the interaction region of the spectrometer. This MW pulse is typically 10-300 ns in duration and temporally overlapped with the beginning of the linearly polarized RF pulse (polarized along the laboratory Y-axis). The RF pulse duration is typically 1-5 μs. The RF pulse is longer than the MW pulse because the RF amplification is lower (100 W for RF vs 300 W for MW). Furthermore, the RF pulse typically excites a purely rotational Q-branch transition, whereas the MW pulse excites a purely rotational P- or R-branch transition. The signal is recorded along the laboratory X-axis. Experiments are performed that excite only a single species or that simultaneously excite multiple species (in this case, conformational isomers). For simultaneously exciting multiple species, the individual MW drive waveforms for each are coadded together to create a composite MW pulse. A composite RF waveform is created from coadding the respective RF twist waveforms. In order to protect the oscilloscope from the full power of the excitation pulses, a switch prevents signal from reaching it until after the excitation pulses are completed. An additional delay is also set on the oscilloscope to avoid recording ringing from triggering and switching events. The experimental setup and timing scheme are shown in Figure 2.

From the measured three-wave mixing signal phases, the enantiomer, i.e., the absolute configuration, can be identified. This task can be accomplished in several ways. One is to first take measurements of samples of a molecule with known excess enantiomer and compare the acquired phases with those from the unknown samples that contain the target molecule. This method is straightforward for molecular species where chirally enriched and characterized samples are available, as we recently showed for an uncharacterized mixture of menthone isomers.[18] A second is to take concurrent measurements involving at least two cycles where the relationship between the absolute phases of the species for the three-wave mixing cycles involved is known. This method was applied in the investigation of carvone.[16] A third way is based on a full characterization of the travel times of signals through the various electronic components and the chamber. Thus, one can predict the absolute phase of the detected signal and compare with the experimental result from a single measurement to determine the absolute configuration. We focus on the first and third methods in this work.

IV. RESULTS AND DISCUSSION

A. Spectral assignment

Figure 3 presents a portion of the rotational spectrum between 5.1 and 5.7 GHz and simulations based on the fitted rotational constants of 4-carvomenthenol. The spectrum contains contributions from three conformations with significant population in the cold conditions of our molecular jet, although several unassigned lines remain that could be due to additional conformers, molecular clusters, contaminants, or instrument noise. Table I summarizes the spectral fitting results and the quantum chemical calculations. The three conformations shown in Table I differ primarily in the rotation of the isopropyl group about the C–C bond connecting the isopropyl group to the cyclohexene ring. The hydroxyl hydrogen points into the cyclohexene ring for all three conformations, giving rise to stabilization through OH-π interactions.

A comparison of the fitted rotational constants to those from the quantum chemical calculations readily allows the assignment of conformation A to structure III. The assignment

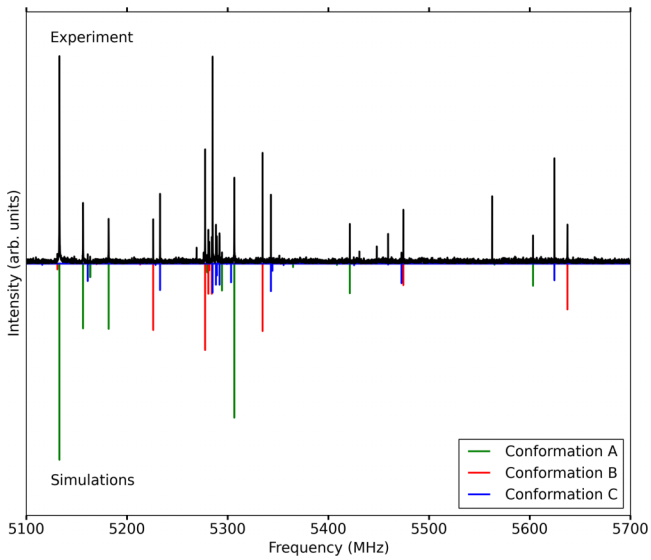

FIG. 3. The rotational spectrum of 4-carvomenthenol between 5.1 and 5.7 GHz. The positive trace is the experimentally obtained spectrum and the negative traces are simulations based on the fitted rotational constants. The experimental spectrum contains contributions from three conformational isomers. Several unassigned lines may be due to additional conformers, molecular clusters, contaminants, or instrument noise.

of conformations B and C is more difficult because the calculated rotational constants are very similar. However, the calculated dipole moment components predict that *b*-type transitions should be stronger for structure II than for structure I. Experimentally, conformation B gives rise to *b*- and *c*-type transitions in a similar intensity ratio to the predicted dipole moment components of structure II. The fact that only five *b*-type transitions were observed for conformation C against 27 and 25 *a*- and *c*-type transitions, respectively, is also in line with the smaller μ_b relative to μ_a and μ_c components predicted for structure I. Furthermore, structure II is predicted to be higher in energy than structure I and, assuming entropic contributions are small, thus should be less populated in the jet, also in agreement with the total number of lines observed for conformations B and C (i.e., fewer lines observed for conformation B relative to conformation C). Thus, conformations B and C are assigned to structures II and I, respectively.

Another important result from the calculations is the signs of the dipole moment components that are required for *a priori* enantiomeric differentiation. The phase of the transition dipole matrix elements for each transition and thus the interaction with the linearly polarized excitation pulses employed here are dependent upon these values. One might expect that low-level calculations are sufficiently accurate to predict the signs, even if the absolute magnitudes are less reliable. However, care should be taken if the magnitudes are small (<0.3 D), because then even small structural changes that can occur between levels of theory can yield different overall signs of the product of the dipole moment components. An example of this can be seen in the relaxed potential energy scan at the M06-2X/6-311++G(d,p) level of theory (Figure 4), where the product of the dipole moment components changed sign near the

TABLE I. Summary of results of spectral fits from SPFIT[29] and quantum chemical calculations. N is the number of lines included into the fit and σ is the standard deviation of the fit. The absolute phase derived from the three-wave mixing experiments is given, along with that expected from the sign of the product of the transition dipole matrix elements. This derivation is discussed in Sec. IV F and in the supplementary material.[22]

	Conformer					
	A (experiment)	III (calculated)[a]	B (experiment)	II (calculated)[a]	C (experiment)	I (calculated)[a]
A (MHz)	2370.3204(13)	2385.5	2255.1848(23)	2271.7	2236.4047(12)	2244.2
B (MHz)	683.174 21(30)	687.7	673.704 63(35)	674.7	674.835 99(26)	681.6
C (MHz)	606.399 55(24)	609.8	646.545 51(32)	652.5	647.304 27(19)	650.2
N (*a*-/*b*-/*c*-type)	60 (39/3/18)	…	49 (29/9/11)	…	57 (27/5/25)	…
σ (kHz)	21.2	…	20.7	…	18.6	…
μ_a (D)[a]	…	−1.43	…	+1.25	…	+1.18
μ_b (D)[a]	…	+0.21	…	+0.72	…	+0.32
μ_c (D)[a]	…	−1.00	…	+0.96	…	−1.17
ϕ_{abs} (rad)	…	…	$\phi_{abs(S)} = -2.68(86)$[b]	$\pm\pi$[c]	$\phi_{abs(S)} = -0.59(84)$[b]	0[c]
			$\phi_{abs(R)} = 0.75(84)$[b]	0[c]	$\phi_{abs(R)} = 2.72(82)$[b]	$\pm\pi$[c]
ΔE (kJ·mol^{-1})[a,d]	…	1.60	…	2.13	…	0.00
Structure[a]	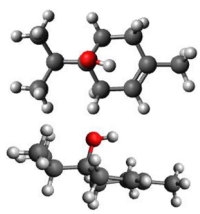		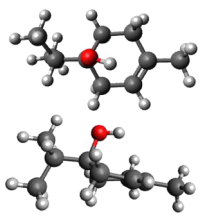		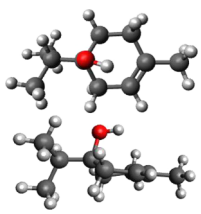	

[a]From M06-2X/6-311++G(d,p) calculations on (*R*)-4-carvomenthenol.
[b]From independent measurements (see Table II).
[c]Derived from the sign of the product of the transition dipole matrix elements, $\mu_X\mu_Y\mu_Z$. See Eqs. (1)–(3) and related discussion.
[d]$\Delta E_i = E_i - E_I$, zero-point corrected.

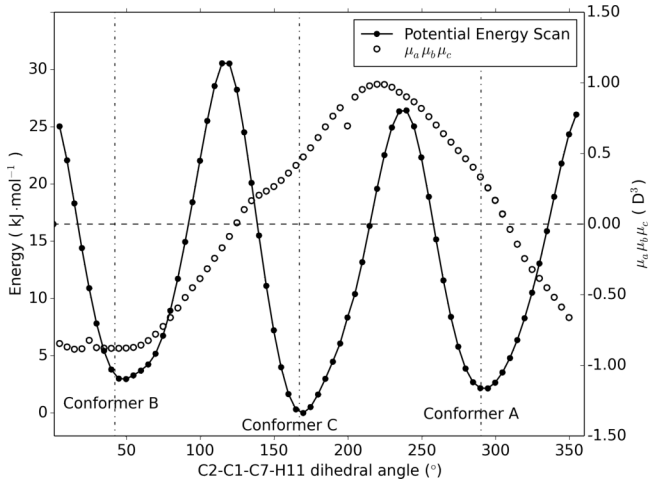

FIG. 4. Relaxed potential energy scan (M06-2X/6-311++G(d,p)) of rotating the isopropyl group about the C–C bond connecting it to the cyclohexene ring, i.e., the dihedral angle formed by the C2–C1–C7–H11 atoms, as labeled in Figure 1. Scans were made on (*S*)-4-carvomenthenol. The B3LYP/6-311++G(d,p) results (not shown here) are very similar to the M06-2X results. The locations of the fully optimized minima are labeled according to the structures given in Table I and indicated with vertical dashed lines. Conformer C is the most stable, although the relative energies of all three structures differ by less than 1.5 kJ/mol. However, relatively high barriers (>20 kJ/mol) separate the conformations. Also of note is the behavior of the sign of $\mu_a\mu_b\mu_c$ (within the principal axis system), which changes within the potential well of conformer A.

conformer A minimum. A full analysis of this result is beyond the scope of this work, but warrants further investigation with higher level theoretical methods and calculations. If one (or more) of the dipole moment components is small, distortions away from the equilibrium structure (e.g., centrifugal distortions, excited vibrations, or zero-point motions) may cause the sign of the small dipole moment component(s) to invert. Such effects have not been considered here, but may be important in other molecules because the three-wave mixing signal obtained would then have an absolute phase opposite from that predicted using the equilibrium structure dipole moment components.

The scan presented in Figure 4 illustrates the differences between the conformations and the potential energy surface on which they exist. All three minima are separated by only about 1.5 kJ/mol. However, the isomerization barriers are relatively high, larger than 20 kJ/mol. We performed further frequency calculations to obtain the zero-point corrections at the M06-2X/6-311++G(d,p) level of theory. These results are summarized in Table I, along with the structural assignments to our experimental spectrum.

Intuitively, the only realistic alternative conformational moieties to the assigned structures are those in which the hydrogen of the OH group points away from the cyclohexene ring rather than into it. However, due to repulsion between the hydroxyl hydrogen and isopropyl group, such structures are expected to have relative energies much higher than those with the OH pointing into the ring. Furthermore, the structures assigned to the observed spectra are stabilized by an OH-π interaction between the OH group and double bond in the cyclohexene ring. In fact, quantum chemical calculations predict that the energy of an optimized structure with the OH rotated away from the ring is 23.4 kJ/mol above that of the local minimum of structure I.

B. Identifying candidate three-wave mixing cycles

Once the spectra are assigned, the fitted molecular constants are used to predict rotational transitions over a wide frequency range. The predictions are made using the program SPCAT.[29] Candidate drive and listen transitions between 2 and 6 GHz are sought that are connected by twist transitions with frequencies between 50 and 550 MHz (limited by the RF amplifier in the current setup). Although the twist transition frequencies are limited to 50-550 MHz, many chiral molecules have transitions within this range and thus can be readily investigated. For a given cycle, the product of the predicted line strengths of all three transitions is obtained as described in Sec. III and compared with other cycles. The cycles with the largest products of the predicted line strengths are the first-choice candidates for the three-wave mixing experiments.

C. RF transition determination

Before attempting the three-wave mixing experiments, we verify the predictions with RF-MW double-resonance experiments. In these experiments, a 2-6 GHz 1 μs long chirp is used for MW excitation along with a scan over the predicted RF transition. Although in our apparatus RF transitions cannot be directly observed, two effects of the RF field near resonance are seen on the intensities and phases of a MW transition with which it shares a common rotational level. One is that the intensity of the MW transition is depleted. The second is that the phase of the MW transition's time-domain signal shifts as the radio frequency approaches resonance, with an inversion of the shift at near perfect resonance. Figure 5 displays these behaviors for scanning the RF over the $J_{K_aK_c} = 3_{13} \rightarrow 3_{12}$ twist transition between 164-166 MHz and monitoring the effect on the $J_{K_aK_c} = 3_{12} \rightarrow 2_{02}$ listen transition at 5624.49 MHz for conformer C. The phase shift at resonance provides a higher resolution value for the transition frequency than the broad intensity depletion. The theory and application of this RF-MW double-resonance method is discussed in a recent publication.[30]

D. Chiral microwave three-wave mixing

Once the twist transitions in the RF range are verified, three-wave mixing is performed with single frequency drive and twist pulses. Using single frequencies for each excitation instead of chirps makes determination of the absolute phase from the observed phase more straightforward.

The cycle employed here is the triad of transitions: $J_{K_aK_c} = 2_{02} \rightarrow 3_{13}$ (drive), $3_{13} \rightarrow 3_{12}$ (twist), and $3_{12} \rightarrow 2_{02}$ (listen) (see energy level diagram of Figure 2). The same cycle is used for conformers B and C, differing only in the transition frequencies. We are unable to observe three-wave mixing on conformer A, likely due to its small μ_b dipole moment component (≈0.2 D, see Table I). Furthermore, calculations predict that the sign of $\mu_a\mu_b\mu_c$ changes near the conformer A minimum (see Figure 4), thus zero-point motions may play

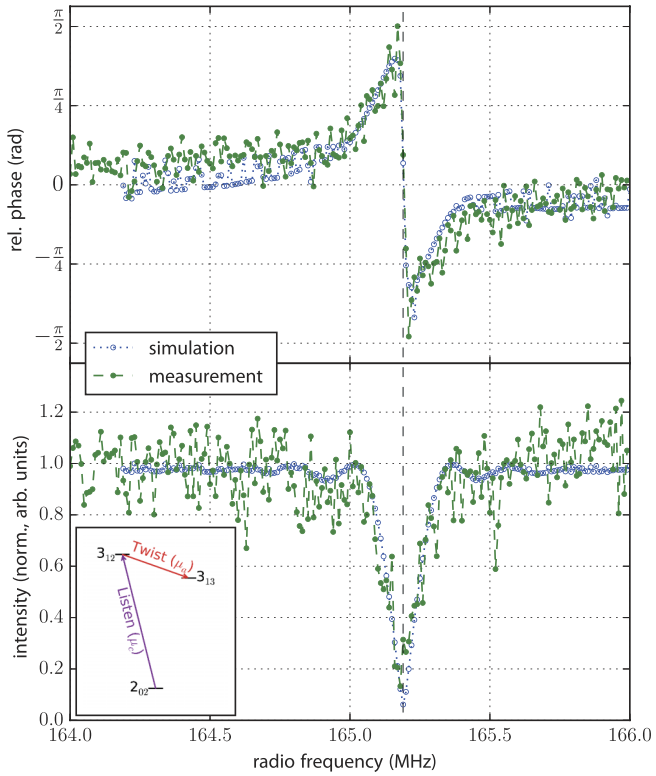

FIG. 5. Results of scanning the radio frequency over the conformer C resonance predicted near 165.19 MHz (twist) and observing the effect on the MW transition at 5624.49 MHz (listen). Simulations are obtained using the three-level optical Bloch equations.[23] The upper traces show the shift in the phase as the RF approaches resonance and the change in sign at near perfect resonance. In the lower traces, the depletion in the signal as the RF passes through resonance is shown. The inset shows the energy level diagram for these transitions. The vertical dashed line indicates the position of the RF resonance.

a role in reducing the signal (i.e., a vibrationally averaged structure with an effective $\mu_b = 0$).

We optimize the three-wave mixing signals for each cycle by varying the MW (10 ns-1.0 μs) and RF (1.0-5.0 μs) pulse durations. For conformer B, pulse durations of 100 ns and 3 μs for the MW and RF pulses yield good results. For conformation C, a MW pulse length of 175 ns is optimal, with good results also from a 3 μs RF pulse. These results of the drive durations are consistent with the calculated magnitudes of the μ_b dipole moment components, 0.72 D and 0.32 D for conformers B and C, respectively. Finer scans of the MW and RF pulse durations could determine the absolute optimal conditions for maximum three-wave mixing signal ($\frac{\pi}{2}$ and π pulses for the drive and twist, respectively[13,23]). However, to simplify the analysis of the phase measurements, we use the same RF durations for all frequencies in experiments where simultaneous measurement of multiple species are performed. An important result from the timing scans is that the phase of the three-wave mixing signal is independent of the length of the pulses, indicating it depends on the initial phases of the excitation fields, so long as the drive and twist pulses remain at or less than π and 2π conditions, respectively (see Table II and the supplementary material[22]). Also of note is that the measured phase was not sensitive to changes in the position, on the order of centimeters, of the valve relative to the excitation and receiving horns and the RF electrodes.

After optimizing the pulse durations, the results from exciting both conformations simultaneously can be compared. The inset of Figure 6 presents the digitally filtered time-domain signals at 5624.49 MHz (the listen frequency for conformation C) for both enantiomers, while Table II presents a summary of the phase measurements. The results from measuring both enantiomers are presented, from both single conformation excitation (independent) and two-conformation simultaneous excitation. Within the uncertainties of the measurements, the phases for a particular enantiomer and conformation are the same for single or multiple conformation excitation. This result is because no change in the phases of the excitation pulses was introduced from coadding the waveforms and the detection scheme also remained unchanged. Furthermore, due to the sign change of the product of the involved transition dipole

TABLE II. Summary of the phases recorded for the conformations B and C and their enantiomers of 4-carvomenthenol. The last column presents results from using coadded excitation pulses with longer durations. The t_0 of the measured phases in this table is when recording of the signal started, i.e., t_r in Figure 2 is set to 0.

		Phase (ϕ)[a]		
Enantiomer	Conformation	Independent[b]	Simultaneous[c]	Simultaneous with longer excitation[d]
(S)	B	−2.05(20)	...	−1.81(48)
	C	−1.74(20)	−1.58(20)	−1.87(28)
(R)	B	1.37(18)	1.38(17)	1.35(04)
	C	1.56(12)	1.98(31)	1.82(20)
$\Delta\phi = \phi_{(S)} - \phi_{(R)}$	B	−3.42(27)	...	−3.16(48)
	C	−3.30(34)	−3.56(37)	−3.69(55)

[a]Phase of listen transition measured at 5637.42 MHz and 5624.49 MHz for conformations B and C, respectively.
[b]Only one conformation at a time was excited. For conformation B, a MW drive pulse at 5474.465 MHz with 100 ns duration was used while for conformation C, the MW drive pulse was at 5459.31 MHz with 175 ns duration. The RF twist frequencies had 3 μs durations at 162.95 MHz and 165.19 MHz for conformations B and C, respectively.
[c]Both conformations were excited concurrently by coadding the excitation waveforms from the independent measurements (i.e., the MW waveforms were coadded together and the RF waveforms were coadded together).
[d]Both conformations were excited concurrently with coadded excitation waveforms with durations increased from those of the independent measurements, i.e., 200 and 350 ns for the drive excitations of conformations B and C, respectively, and RF durations increased to 5 μs.

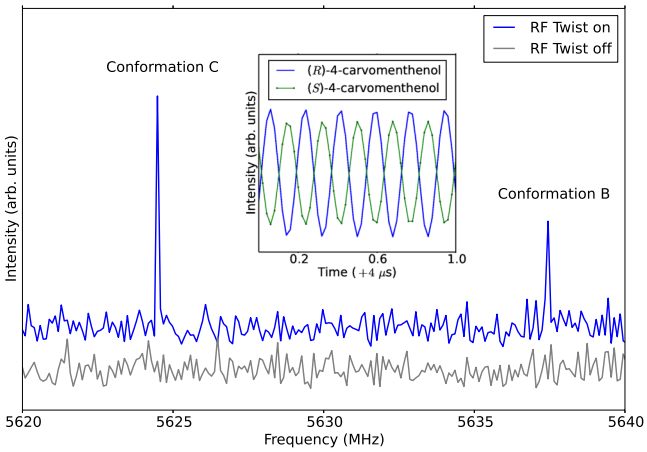

FIG. 6. Portion of the MW spectrum containing the listen transitions of conformations B and C of (*R*)-4-carvomenthenol. The MW excitation pulses were coadded, with durations of 200 and 350 ns at frequencies of 5474.465 and 5459.31 MHz for conformations B and C, respectively. The RF excitation pulses were also coadded, both 3 μs in durations with frequencies of 162.95 and 165.19 MHz for conformations B and C, respectively. The upper trace shows the spectrum with the RF twist on such that three-wave mixing can occur while the lower trace shows that no three-wave mixing signal is present when the RF twist is off. The inset presents a 1 ns portion of the digitally filtered time-domain signal of the listen frequency at 5624.49 MHz of conformation C for both enantiomers. The π radian shift between the signals is clearly seen.

matrix elements, a phase shift of π radians is observed between the signal phases from opposite enantiomers. This phase shift between enantiomers is the signature that allows us to unambiguously differentiate the enantiomers and to determine which is in excess.

To further illustrate the robustness of measuring multiple species simultaneously, Figure 6 presents the portion of the MW spectrum covering both listen frequencies for conformations B and C observed from simultaneous excitation. Such results demonstrate the power of this high-resolution technique to identify chiral molecules in mixtures. Molecules as similar as conformational isomers can be simultaneously excited and their enantiomers differentiated by using conformation-specific resonances, even in cases where the individual conformations have opposite signs of the product of their transition dipole matrix elements. Furthermore, even mixtures containing molecules with opposite optical rotations can be easily and separately measured. The number of species that can be simultaneously measured is limited by the resolution of the instrument, i.e., the individual listen transitions must remain resolvable from each other. In the experiments recording 10 μs of the FID, the frequency resolution was 100 kHz. Furthermore, the phase of the observed signals may be influenced if the drive or twist signals of two different cycles are close in frequency (within 5 MHz of each other). This influence depends on the powers and durations of the excitation pulses and merits further investigation.

E. Enantiomeric excess

An important application of the microwave-three wave mixing experiment is the determination not only of the excess enantiomer but also by how much it is in excess. Enantiomeric excess is defined as $ee = |f_1 - f_2|$, where f_1 and f_2 are the fractions of each enantiomer present in the mixture and $f_1 + f_2 = 1$. This application arises from the linear dependence of the signal intensity on the *ee* (see Eq. (1)). Thus, if one has a measurement of a sample of known *ee*, e.g., an enantiopure sample, then the *ee* of unknown samples can be determined by direct comparison.[18]

The 4-carvomenthenol samples we obtained from Sigma-Aldrich had a stated *ee* of 0.33 ± 0.08 (uncertainty computed from the reported $[\alpha]_D^{20} = -25° \pm 6°$ value) for both the (*R*) and (*S*) samples. Assuming an *ee* of 0.33 for the (*R*)-4-carvomenthenol sample and comparing the three-wave mixing intensities of the (*R*)- and (*S*)-4-carvomenthenol samples, we obtain *ee* values of 0.30 ± 0.06 for the (*S*)-enantiomer and an uncertainty of ±0.07 for the (*R*)-enantiomer. These *ee* values and uncertainties (statistical errors) are obtained by comparison of integrated frequency domain listen intensities over the relevant transitions. The integrated signal of the drive transition with the RF turned off is used as an internal reference to account for fluctuations in experimental conditions between different experimental runs. In an independent gas chromatography measurement by the group of Oliver Trapp at the University of Heidelberg, the (*S*)-4-carvomenthenol sample had an *ee* = 0.38 and the (*R*)-4-carvomenthenol sample had an *ee* = 0.40,[31] in qualitative agreement with our measurements. In total, the three-wave mixing *ee* measurement for each enantiomer required approximately 4 h, the time needed to obtain 75 000 acquisitions each (150 000 in total) at 10 Hz for both the three-wave mixing listen and RF off drive signals. These times can be reduced with fully optimized excitation pulses and by further increasing the experimental duty cycle.

We prepared a mixture of (*R*)-4-carvomenthenol with *ee* = 0.049 ± 0.008, where the uncertainty primarily arises from the accuracy of the balance used to prepare the mixture. The phase of the signal from this measurement of conformation C was 1.44(37) rad, agreeing very well with that measured for the 0.33 *ee* (*R*)-4-carvomenthenol (1.56(12) rad, see Table II). From the signal intensities, we obtained an *ee* of 0.058 ± 0.02.

F. Absolute configuration

If one knows the timings of the excitation pulses and listen signals through the different parts of the apparatus, then a single measurement of the phase and knowledge of the transition dipole matrix elements are sufficient to identify the absolute configuration of the excess enantiomer. This condition is difficult to achieve in practice because the effects of each electronic component on the excitation and response signals must be considered. The primary sources of dispersion in our apparatus are the horn antennas, for which the delay as a function of frequency has been previously modeled.[32] The supplementary material[22] presents a plot of the transit time of signals through our chamber as a function of frequency. The important result from this plot is that in the region of the drive and listen frequencies used here, the transit times are flat, differing by at most 12 ps between 5.45 and 5.65 GHz. We thus make the approximation that all transit times within this narrow frequency range are equal. This approximation introduces an error in the derived absolute phases of at most

0.41 rad at the highest listen frequency employed here. In order to confidently differentiate the enantiomers, an error of at most 1 rad is a reasonable target. The accuracy to which the transit times must be measured at 6 GHz is then 26.5 ps = $\frac{1\text{ rad}}{2\pi \cdot 6\text{ GHz}}$. Extension to higher frequencies requires more accurate transit time measurements, e.g., 13.3 ps at 12 GHz. Furthermore in cases where the drive and listen frequencies are more greatly separated, the effect of the differing transit times must be considered.

A value of t_r = 4539.80(2) ns for $t = t_r$ in Eq. (1) was obtained via measurements of the transit times of MW pulses through the apparatus. The initial phases of the excitation pulses are contained within Eq. (1) and were set to 0 rad on the AWG. However, the RF and MW pulses take separate paths (i.e., through two different amplifiers and cables of different types and lengths) and thus arrive at the molecular interaction region at different times. Since the RF pulse arrives first, we must determine its phase at the time that the MW pulse arrives, i.e., $\phi_{s,RF} = -2\pi\nu_{s,RF}t_{delay}$ where t_{delay} is the delay between the arrival of the RF and MW pulses and $\nu_{s,RF}$ is the frequency of the RF pulse for conformer s. Our timing measurements determine that t_{delay} = 13.13(2) ns. As $\phi_{MW} = 0$, for enantiomer e of conformer s, the observed phase from Eq. (1) is given in the following:

$$\phi_{obs(s,e)} = -2\pi\nu_s t_r + \phi_{s,RF} + \phi_{abs(s,e)}. \quad (4)$$

The absolute phase is $\phi_{abs(s,e)}$ and in this formulation can take values of 0 or $\pm\pi$. Careful consideration of the transition dipole matrix elements must be made in attempts to assign the absolute configuration as it is the absolute phase that allows one to determine which enantiomer is in excess in the measured sample. Note that Eq. (4) differs from that employed in our previous work on carvone[16] in that it contains a separate $\phi_{s,RF}$ term while in the carvone work, the RF phase was included in the absolute phase term. Furthermore, we used chirped drive pulses in our carvone work, but the method described here using single-frequency excitations is more rigorous and general.

By rearranging Eq. (4), we obtain an expression for the absolute phase,

$$\phi_{abs(s,e)} = \phi_{obs(s,e)} + 2\pi(\nu_s t_r + \nu_{s,RF}t_{delay}). \quad (5)$$

By applying Eq. (5), we obtain experimental absolute phases of $\phi_{abs(B,S)} = -2.68(86)$, $\phi_{abs(B,R)} = +0.75(84)$, $\phi_{abs(C,S)} = -0.59(84)$, and $\phi_{abs(C,R)} = +2.72(82)$. These absolute phases agree with those predicted using the transition dipole matrix elements calculated with PGOPHER[33] (see the supplementary material[22]) using the dipole moment components within the principal axis system obtained from quantum chemical calculations (see Table I).

For the three-wave mixing cycle employed herein ($J_{K_aK_c} = 2_{02} \rightarrow 3_{13}$ (drive), $3_{13} \rightarrow 3_{12}$ (twist), and $3_{12} \rightarrow 2_{02}$ (listen)), the geometry of our apparatus projects the b-type drive transition onto the laboratory Z-axis (with $\Delta M = 0$), the a-type twist transition onto the laboratory Y-axis (with $\Delta M = \pm 1$), and the c-type listen transition is observed polarized along the laboratory X-axis (with $\Delta M = \mp 1$). For this cycle in (*S*)-4-carvomenthenol, the different possible products of the three transition dipole matrix elements, $\mu_X\mu_Y\mu_Z$, for all allowed transitions between M levels (and yielding a total $\Delta M = 0$ for the complete cycle) were all positive for conformation B and negative for conformation C. The asymmetric top transition dipole matrix elements were computed using PGOPHER[33] and their values are given in the supplementary material.[22] Although the uncertainties in the measured phases are large, they are more than adequate to unambiguously differentiate the enantiomers. It is worth noting once more that the π radian phase difference between enantiomers means that one can easily identify the excess enantiomer in a mixture, even if the derived absolute phase from the unknown sample has a large uncertainty (e.g., 1 rad). Thus, with the aid of quantum chemical calculations and evaluation of the transition dipole matrix elements, we can determine the absolute configuration of the excess enantiomers within these samples.

As mentioned previously, another method for determining the absolute configuration is comparative measurements with known samples. Such comparisons require measurements of samples with known excess enantiomer in order to determine the absolute configuration of an unknown mixture. For example, the three-wave mixing signal phases for conformation C from the 5% *ee* mixture we prepared (ϕ = +1.44(37) rad) and that of the (*R*)-4-carvomenthenol sample with a reported 33% excess (ϕ = +1.56(12) rad) agree very well; thus, the absolute configuration of the mixture could be assigned as (*R*)-4-carvomenthenol. Note that these comparisons make use of the measured phases, not the absolute phases.

V. SUMMARY AND CONCLUSIONS

In this work, we reported the rotational spectrum of 4-carvomenthenol and observed the presence of three conformations in our supersonic expansions. From fits of the rotational spectrum and comparison with quantum chemical calculations, we assigned structures to the experimentally determined sets of rotational constants. The structures were all stabilized by intramolecular OH-π interactions and differed only in rotation of the isopropyl group relative to the cyclohexene ring. The magnitudes of the computed dipole moment components and relative conformational energies were used to distinguish conformers B and C, as their rotational constants were very similar.

Prior to performing three-wave mixing experiments, we optimized the excitation pulses for maximum signal. To this end, we made coarse pulse duration scans of the RF and MW pulses. We found that the MW pulse durations agreed qualitatively with the magnitudes of the computed dipole moment components.

Three-wave mixing experiments were successful on conformations B and C. We attempted three-wave mixing on conformation A but did not observe signal above the noise level, likely due to its small μ_b dipole moment component. We used the results of these experiments to compare with a prepared mixture with an *ee* of less than 10%. However, *ee* measurements will still require comparison to known standards, but the comparison values could be tabulated and thus would not need to be measured each time.

The transition dipole matrix elements for each transition in the three-wave mixing cycle were calculated using

PGOPHER.[33] The products, $\mu_X\mu_Y\mu_Z$, of these matrix elements were used to predict the absolute phases of the three-wave mixing signals. Therefore, we could conclude that extraction of the absolute configuration from the measured phase of a single measurement was possible. This extraction required only knowledge of the derived dipole transition matrix elements (with the aid of the dipole moment components along the principal axes from quantum chemical calculations) and signal transit times through the instrument. For the cycles studied here, and in other molecules not reported herein, this method of determining the absolute configuration has been successful. However, more work is still needed to verify that it is completely general. Other effects or dependences (e.g., dependence on K, centrifugal distortion, or zero-point motions) could also influence the absolute phase. Future work is aimed towards investigating more asymmetric molecules in order to gain insight into the relation between the observed phase and absolute configuration.

ACKNOWLEDGMENTS

We acknowledge fruitful discussions with Cristobal Perez. D.S. acknowledges use of the GWDG computing cluster. Funding of the Deutsche Forschungsgemeinschaft is acknowledged (Sachbeihilfe SCHN1280/1-1). M.S. acknowledges financial support from the Fonds der Chemischen Industrie via a Dozentenstipendium. This work was supported by the excellence cluster "The Hamburg Centre for Ultrafast Imaging — Structure, Dynamics, and Control of Matter at the Atomic Scale" of the Deutsche Forschungsgemeinschaft for which D.P. also acknowledges for travel support.

[1]L. Wade, *Organic Chemistry*, 3rd ed. (Prentice Hall, New York, 1995).
[2]H. P. Latscha, U. Kazmaier, and H. A. Klein, *Organische Chemie*, 6th ed. (Springer, Berlin, 2008).
[3]J. Gal, Chirality **12**, 959–976 (2012).
[4]T. J. Leitereg, D. G. Guadagni, J. Harris, T. R. Mon, and R. Teranishi, J. Agric. Food Chem. **19**(4), 785 (1971).
[5]J. Hyttel, K. Bøgesø, J. Perrgaard, and C. Sánchez, J. Neural Transm. **88**(2), 157–160 (1992).
[6]N. Böwering, T. Lischke, B. Schmidtke, N. Müller, T. Khalil, and U. Heinzmann, Phys. Rev. Lett. **86**, 1187–1190 (2001).
[7]L. Nahon, G. A. Garcia, C. J. Harding, E. Mikajlo, and I. Powis, J. Chem. Phys. **125**(11), 114309 (2006).
[8]G. A. Garcia, L. Nahon, M. Lebech, J.-C. Houver, D. Dowek, and I. Powis, J. Chem. Phys. **119**(17), 8781–8784 (2003).
[9]C. Lux, M. Wollenhaupt, T. Bolze, Q. Liang, J. Köhler, C. Sarpe, and T. Baumert, Angew. Chem., Int. Ed. **51**(20), 5001–5005 (2012).
[10]M. H. M. Janssen and I. Powis, Phys. Chem. Chem. Phys. **16**, 856–871 (2014).
[11]M. Pitzer, M. Kunitski, A. S. Johnson, T. Jahnke, H. Sann, F. Sturm, L. P. H. Schmidt, H. Schmidt-Böcking, R. Dörner, J. Stohner, J. Kiedrowski, M. Reggelin, S. Marquardt, A. Schießer, R. Berger, and M. S. Schöffler, Science **341**(6150), 1096–1100 (2013).
[12]D. Patterson and M. Schnell, Phys. Chem. Chem. Phys. **16**, 11114–11123 (2014).
[13]S. Lobsiger, C. Perez, L. Evangelisti, K. Lehmann, and B. Pate, J. Phys. Chem. Lett. **6**(1), 196–200 (2015).
[14]D. Patterson, M. Schnell, and J. Doyle, Nature **497**, 475–477 (2013).
[15]D. Patterson and J. Doyle, Phys. Rev. Lett. **111**, 023008 (2013).
[16]V. Shubert, D. Schmitz, D. Patterson, J. Doyle, and M. Schnell, Angew. Chem., Int. Ed. **53**, 1152–1155 (2014).
[17]E. Hirota, Proc. Jpn. Acad., Ser. B **88**(3), 120–128 (2012).
[18]V. Shubert, D. Schmitz, and M. Schnell, J. Mol. Spectrosc. **300**, 31–36 (2014).
[19]K. A. Hammer, C. F. Carson, and T. V. Riley, Antimicrobrial Agents Chemother. **56**(2), 909–915 (2012).
[20]N. Pazyar, R. Yaghoobi, N. Bagherani, and A. Kazerouni, Int. J. Dermatol. **52**(7), 784–790 (2013).
[21]V. Schurig, U. Leyrer, and U. Kohnle, Naturwissenschaften **72**(4), 211 (1985).
[22]See supplementary material at http://dx.doi.org/10.1063/1.4921833 for linelists and mathematical derivations.
[23]J.-U. Grabow, Angew. Chem., Int. Ed. **52**, 11698–11700 (2013).
[24]G. W. King, R. M. Hainer, and P. C. Cross, J. Chem. Phys. **11**(1), 27 (1943).
[25]A. Bauder, *Handbook of High-Resolution Spectroscopy* (John Wiley & Sons, Ltd., 2011).
[26]D. Schmitz, V. A. Shubert, T. Betz, and M. Schnell, J. Mol. Spectrosc. **280**, 77–84 (2012).
[27]G. G. Brown, B. C. Dian, K. O. Douglass, S. M. Geyer, S. T. Shipman, and B. H. Pate, Rev. Sci. Instrum. **79**(5), 053103 (2008).
[28]M. J. Frisch, G. W. Trucks, H. B. Schlegel, G. E. Scuseria, M. A. Robb, J. R. Cheeseman, G. Scalmani, V. Barone, B. Mennucci, G. A. Petersson, H. Nakatsuji, M. Caricato, X. Li, H. P. Hratchian, A. F. Izmaylov, J. Bloino, G. Zheng, J. L. Sonnenberg, M. Hada, M. Ehara, K. Toyota, R. Fukuda, J. Hasegawa, M. Ishida, T. Nakajima, Y. Honda, O. Kitao, H. Nakai, T. Vreven, J. A. Montgomery, Jr., J. E. Peralta, F. Ogliaro, M. Bearpark, J. J. Heyd, E. Brothers, K. N. Kudin, V. N. Staroverov, R. Kobayashi, J. Normand, K. Raghavachari, A. Rendell, J. C. Burant, S. S. Iyengar, J. Tomasi, M. Cossi, N. Rega, J. M. Millam, M. Klene, J. E. Knox, J. B. Cross, V. Bakken, C. Adamo, J. Jaramillo, R. Gomperts, R. E. Stratmann, O. Yazyev, A. J. Austin, R. Cammi, C. Pomelli, J. W. Ochterski, R. L. Martin, K. Morokuma, V. G. Zakrzewski, G. A. Voth, P. Salvador, J. J. Dannenberg, S. Dapprich, A. D. Daniels, O. Farkas, J. B. Foresman, J. V. Ortiz, J. Cioslowski, and D. J. Fox, GAUSSIAN 09, Revision A.1, Gaussian, Inc., Wallingford, CT, 2009.
[29]H. M. Pickett, J. Mol. Spectrosc. **148**, 371–377 (1991).
[30]D. Schmitz, V. A. Shubert, D. Patterson, A. Krin, and M. Schnell, J. Phys. Chem. Lett. **6**, 1493–1498 (2015).
[31]O. Trapp, personal communication (2014).
[32]J. D. McKinney, D. Peroulis, and A. M. Weiner, IEEE Trans. Antennas Propag. **56**(1), 39–47 (2008).
[33]C. Western, PGOPHER (beta version 8.0.326), a program for simulating rotational structure, 2015.